Epitaxial growth of Fe(001) on $CoSi_2$(001)/Si(001) surfaces: Structural and electronic properties

P. Bertoncini, P. Wetzel,* D. Berling, and G. Gewinner
Laboratoire de Physique et de Spectroscopie Electronique, UPRES, A 7014 CNRS, 4 rue des Frères Lumière, 68 093 Mulhouse Cedex, France

C. Ulhaq-Bouillet and V. Pierron Bohnes
Institut de Physique et de Chimie des Matériaux de Strasbourg-Groupe d'Etudes des Matériaux Métalliques, 23, rue du Loess, 67037 Strasbourg Cedex, France

(Received 13 May 1999)

Ultrathin Fe films, in the thickness range 0–40 monolayers (ML), have been grown on Si(001) by molecular-beam epitaxy and characterized by low-energy electron diffraction, inelastic medium-energy electron diffraction, x-ray photoelectron spectroscopy, angular-resolved ultraviolet spectroscopy, x-ray photoelectron diffraction, ion scattering spectroscopy, and transmission electron microscopy. For Fe depositions onto Si(001) at room temperature, a disordered layer is obtained due to a high degree of intermixing between the Fe deposit and the Si substrate. Successful epitaxial growth of Fe at room temperature is achieved by use of a thin (~10 Å) $CoSi_2$ silicide interlayer epitaxially grown on the Si(001) substrate prior to the Fe deposition, which prevents the intermixing of the Si substrate atoms into the Fe overlayer. Below a coverage of ~2 ML, a reacted ordered iron-rich phase forms at the surface. At higher coverages, there is growth of an epitaxial essentially body-centered cubic (bcc) Fe(001) overlayer with the orientational relationships $Fe(001)\langle 001\rangle \| CoSi_2(001)\langle 001\rangle \| Si(001)\langle 001\rangle$. Finally, a well-ordered Fe/$CoSi_2$ interface is formed even at room temperature. [S0163-1829(99)12335-X]

I. INTRODUCTION

The ability to grow high-quality magnetic epitaxial thin films of $3d$ metals on semiconductor single crystal is an important field, since for many technological applications as well as for fundamental physics studies one wants to exploit the magnetic anisotropy of the material. On the other hand, the growth of magnetic thin films offer unique opportunities for exploring the correlation between atomic structure and magnetic properties in these systems.

The Fe-Si system is of great interest due to the possible incorporation of magnetic elements into silicon-integrated optoelectronic or microelectronic devices. A number of investigations dealing with the interlayer coupling in Fe-Si multilayers have been reported.[1–4] However, concerning the spacer, its nature metallic or semiconductor is poorly understood, and it is not well established how it affects the coupling in the Fe-Si multilayers.

Several structural and magnetic studies of Fe on Si(001) at room temperature[5–8] (RT) have already been reported. However, it has been observed that a spontaneous and significant chemical intermixing occurs between the Fe transition-metal overlayer and the semiconductor Si substrate. The first-deposited Fe atoms react with the surface by forming an ~20–30-Å-thick amorphous Fe_xSi_{1-x} silicide-like overlayer. For subsequent Fe deposits the reaction slows down probably due to the diffusion barrier through the interfacial disordered silicide layer and the Si dissolution in the overlayer diminishes. Thus, a metallic disordered Fe layer develops. The Fe-Si interfacial interdiffusion can be reduced by lowering the temperature of the substrate during the Fe evaporation. By this way, sharper interfaces between the substrate and the overlayer are obtained but the resulting Fe films are found to be highly defected with rough surfaces.[5,9] The Si interdiffusion of the RT as-grown Fe films is known to have strong influence on its magnetic behavior.

Recently, we have reported the connection between the structure and the magnetism on epitaxial Fe_xSi_{1-x} $(0.5<x<1)$ films grown on Si(111) at RT.[10] Magneto-optic Kerr effect (MOKE) measurements showed an increase of the magnitude of the uniaxial anisotropy constant with increasing Si concentration. Furthermore, x-ray magnetic circular dichroism measurements indicated a diminution of the local magnetic moment on the Fe atoms with increasing the Si concentration in the layer. So, the presence of Si in the Fe layer strongly affects ferromagnetism and is found to quench it completely in the FeSi stoichiometry.[10]

In order to obtain sharper semiconductor-metallic interfaces and to better control the nature of the interface, it is desirable to prevent outdiffusion of Si by a barrier layer. Moreover, it is noteworthy that body-centered cubic (bcc) Fe and Si crystals have closely related lattice parameters $a_{Si} \cong 2a_{Fe}$ with a misfit of 5.6%, which suggests that α-Fe may be epitaxially grown on Si(001). Here, we have chosen as one such possibility a $CoSi_2$ silicide layer. $CoSi_2$ crystallizes in the CaF_2 structure with very close lattice match to Si (1.2%) and is known to be of high-crystalline quality when grown epitaxially on Si(111).[11–13] Previous studies[14–17] have also demonstrated that single-orientation epitaxial $CoSi_2$(001) films can be grown on top of Si(001) in the CaF_2 cubic-crystal structure. The $CoSi_2$ silicide is metallic but presents no magnetic ordering.

In this study, we have employed low-energy electron diffraction (LEED), inelastic medium-energy electron diffraction (IMEED), x-ray photoelectron spectroscopy (XPS), angular-resolved ultraviolet spectroscopy (ARUPS), x-ray photoelectron diffraction (XPD), ion scattering spectroscopy (ISS), and transmission electron microscopy (TEM) techniques to determine the atomic and electronic structure of Fe ultrathin films grown on $CoSi_2$(001)/Si(001) surfaces at RT. It is shown that the addition of an ultrathin-ordered silicide layer (~10 Å) on top of the Si(001) surface prior to Fe growth can drastically change the growth mode of this system. We demonstrate that nearly pure epitaxial bcc Fe can be formed on Si(001) by use of thin-$CoSi_2$ silicide template layers epitaxially grown on Si(001) substrates. This epitaxial interlayer acts as a seed and enables the epitaxial growth of essentially bcc Fe at RT, with sharp interfaces, and also serves as a diffusion barrier of Si substrate atoms in the Fe overlayer, thereby decreasing drastically the Si concentration in the Fe overlayer. This is the first demonstration of epitaxial Fe(001) layer growth on Si(001) substrate at RT.

II. EXPERIMENT

Sample preparation and all measurements, with exception of TEM, were performed in a two-chambers ultrahigh vacuum (UHV) system including a molecular-beam epitaxy (MBE) preparation chamber and an analysis chamber equipped with facilities for LEED, IMEED, XPD, XPS, ARUPS, and ISS techniques. The base pressure of the individual chamber was better than 10^{-10} mbar.

The Si(001) substrates were cleaned by cycles of Ar^+ sputtering and followed by annealing to 850 °C. This treatment produced contamination free surfaces with a high degree of crystallographic order with a long coherence length as attested by sharp (2×1) two-domain LEED patterns.

The $CoSi_2$ template layer was grown on Si(001) by deposition at RT of a thin (4 ML) film of Co followed by heating to 400 °C for 30 min. This produces a fairly well-ordered single-domain $CoSi_2$ film with the (001) orientation, which exhibits a sharp $c(2\times2)$ $(\sqrt{2}\times\sqrt{2}\mathrm{R}45°)$ LEED pattern. In previous studies,[17,18] it was proposed that, $CoSi_2$ layers prepared in such way, are arranged in the CaF_2 structure terminated by a Si layer with an additional half monolayer of Si atoms in a $c(2\times2)$ arrangement.

The Fe films were deposited onto substrates by MBE at a rate of ~ one monolayer (ML) per minute from an Al_2O_3 crucible of a knudsen cell. The deposition rate was monitored by a quartz-oscillator thickness monitor. Here, we define one ML of Fe as the atomic density of a single bcc Fe(001) monolayer ($1\ \mathrm{ML}=1.2\ 10^{15}$ atoms/cm^2) which is twice that of the Si(001) surface. The substrate temperature was held at RT. During growth the background pressure remained always below 2.10^{-10} mbar.

For the *ex situ* TEM analysis, the films were capped with a nonmagnetic FeSi layer (~20 Å) and a Si layer (~20 Å) to protect them from oxidation prior to removal of the completed sample from the growth chamber. The FeSi capping layer grows epitaxially on the Fe-deposited layers by coevaporation of Fe and Si at RT in stoichiometric ratio. The TEM samples were prepared by mechanical thinning (tripod method).

All *in situ* experiments were conducted using a Leybold EA200 spectrometer equipped with a 150-mm radius hemispherical analyzer, selectable angular resolution from ±1° to ±8°, and a multichannel detector with 18 discrete channels capable of high-count rate. The measurements of the photoelectron diffraction modulations of the Fe2$p_{3/2}$ core line at a kinetic energy of 779 eV, were performed with an unmonochromatized Alk_α radiation ($h\nu=1486.6$ eV). Polar angular scans along the two principal azimuths, [100] and [110], in the $CoSi_2$(001) surface plane, were recorded by rotating (angle θ) the sample in a geometry with a fixed angle between the incidence photons and the photoelectron collection directions. The polar angle θ is referred to the surface normal of the sample. The ARUPS experiments were done using a standard He discharge lamp. The XPD and ARUPS angular resolutions of the electron detector were set to ±1°. In XPS, monochromatized Alk_α radiation was used to measure the Fe2$p_{3/2}$ core lines. With the same analyzer in constant retard ratio mode the ISS spectra were recorded using a primary He^+ beam of 1000 eV kinetic energy. The incidence angle and the emission angle could be varied but the scattering geometry (scattering angle=130°) was kept fixed. The acceptance angle in ISS was set to the maximum value of ±8°. IMEED maps were collected at a primary energy of 900 eV by means of a conventional LEED optics.

Electron microscopy was performed employing a TOPCON EM 0023 microscope operating at a beam voltage of 200 kV.

III. RESULTS AND DISCUSSION

LEED results

The surface order and morphology of Fe/$CoSi_2$(001)$c(2\times2)$ is investigated by means of LEED. The LEED pattern of the $CoSi_2$(001) surface shows a very clear and sharp $c(2\times2)$ reconstruction indicating a very flat and well-crystallized surface with typical terrace widths larger than the LEED beam coherence (~200 Å). When Fe is deposited at RT onto the clean $CoSi_2$(001) surface the $c(2\times2)$ spot intensity slowly decreases and the LEED pattern gradually evolves into a (1×1) periodicity. The $c(2\times2)$ spots vanish after deposition of 4–5 ML of Fe and only the (1×1) integral order spots are now visible indicating the pseudomorphic growth of a well-ordered phase with the (1×1) periodicity. One point of interest is that the (1×1) spots show specific intensity profiles, which exhibit periodic variations of their width and intensity distribution with increasing electron energy even for deposit as small as 1 ML of Fe. These oscillations of the width of LEED (1×1) spots with incident electron energy are explained in terms of constructive and destructive interferences of the electron wave function reflected from the (001) terraces, which are separated by monoatomic steps.[19,20] This is consistent with the growth of films with rough surfaces, i.e., surface morphologies with a high density of steps. The LEED spot widths at an out-of-phase condition, which allows us to estimate the average terrace width, indicate mean step separations of the thin-film surface of typically ~10 Å. At large thicknesses (≥40 ML) the LEED show an increased background intensity and a reduction of the (1×1) spot intensity, suggesting a poorer

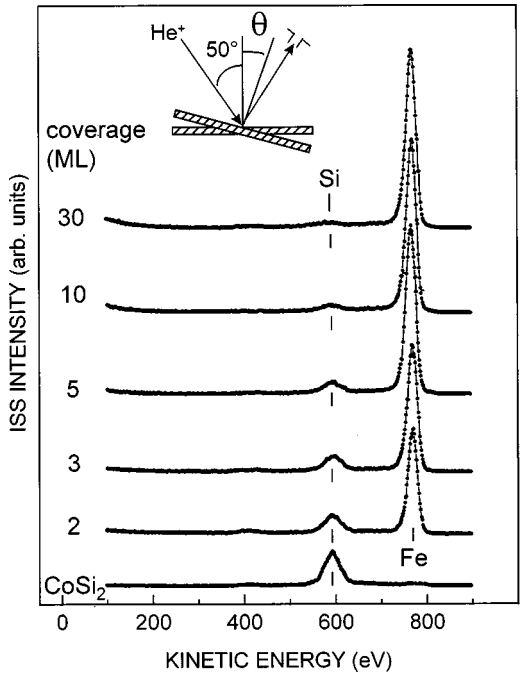

FIG. 1. Ion scattering spectroscopy (ISS) spectra recorded during Fe deposition on $CoSi_2(001)$ at room temperature. The inset shows a schematic view of the geometrical conditions. The scattered He^+ ions are detected at a fixed angle of ~130°.

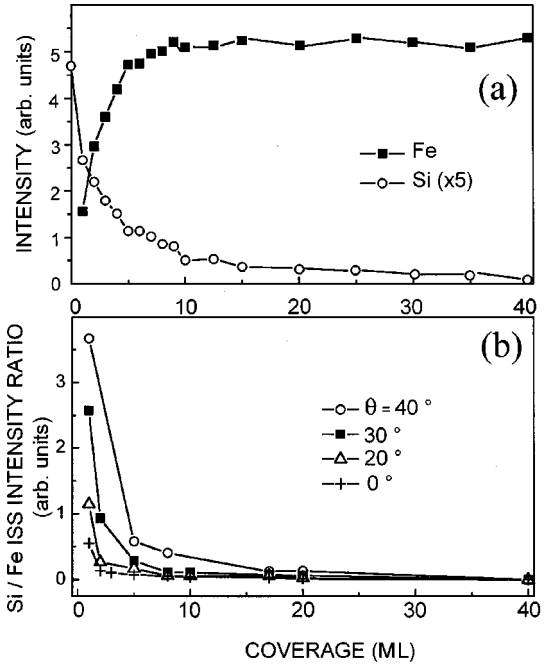

FIG. 2. (a) Evolution of the Fe and Si ISS peaks intensity as a function of Fe coverage. The Si peak intensity is multiplied by 5 to facilitate the comparison with the Fe signal. (b) Ratio of the Si and Fe ISS intensities as a function of Fe coverage for different angle of incidence (θ) of the He^+ ions.

long-range order of the growing films. No indications for faceting can be detected by LEED.

Finally, the LEED patterns show that Fe layers grown at RT are epitaxial on $CoSi_2(001)$ surfaces, despite the large lattice mismatch of the two materials (~7%), while they are polycrystalline on Si(001). The stepped Fe surfaces during the growth seem to be connected with the limited diffusion length of the Fe adatoms at RT. The surface topography should be examined with scanning tunneling microscopy (STM) in order to obtain a better idea of the level of surface roughness exhibited.

ISS results

In order to determine the chemical identity of the atoms at the surface as the interface is formed, ISS measurements were carried out during the Fe deposition. In ISS, the inelastically scattered ions are analyzed, and information on the atomic species in the topmost or two topmost atomic layers at the surface can be obtained by considering how the kinetic energy of the incident ions is divided between the scattered atoms and the substrate atoms. Figure 1 shows ISS spectra recorded at various Fe coverages. The inset displays a scheme of the geometrical conditions for data recording. The clean $CoSi_2(001)$ surface spectrum shows only a peak at ~591 eV kinetic energy corresponding to Si atoms. This observation points out that at least one or more Si topmost atomic layers terminate the $CoSi_2(001)$ surface, in good agreement with the surface structure model suggested in the literature.[17,18] Fe deposition gives rise to a new peak at ~760 eV kinetic energy corresponding to Fe species. Figure 2(a) shows the Si and Fe ISS intensity variation upon deposition of the Fe onto the $CoSi_2(001)$ surface. As is apparent, the Fe intensity rapidly increases, whereas the Si rapidly decreases upon Fe deposition. One can see that for ~10-ML Fe deposit, the Fe signal reached its maximum intensity while a very weak signal from Si (~5%) is still detected under these conditions. The Si signal completely disappears for ~40 ML. The ISS data recorded during the early stages of Fe deposition (coverage below 10 ML) clearly excludes the formation of a pure Fe or Si termination. It can be seen in Fig. 2(a) that deposition of ~2 ML of Fe corresponds to about 60% of the intensity of a single-bcc Fe(001) layer while the fraction of Si at the surface can be estimated to be ~40%. We can interpreted this result in terms of either intermixing or formation of three-dimensional Fe islands with segregated Si. The measurement of the Si to Fe ISS intensity ratio as a function of angle of incidence shown in Fig. 2(b) clearly indicates that Si segregation certainly takes place since strong shadowing of the Fe is seen at grazing incidence. For coverages above 5 ML, a largely unreacted Fe overlayer forms on top of the intermediate layer, while substantial Si segregation is seen at coverages up to 40 ML.

A comparison with results obtained for 10 ML of Fe deposited at RT onto $CoSi_2(001)/Si(001)$ and Si(001) shows a Si signal three times greater and points to much larger intermixing and segregation phenomena in the Fe/Si(001) than in the $Fe/CoSi_2(001)/Si(001)$ system.

IMEED results

Structural information concerning the growth of $Fe/CoSi_2(001)$ can be quickly obtained by inelastic medium-energy electron diffraction (IMEED). IMEED is based on the fact that inelastic backscattered electrons in the KeV range show strong enhancement of intensity along directions defined by atomic rows, because of the forward scattering

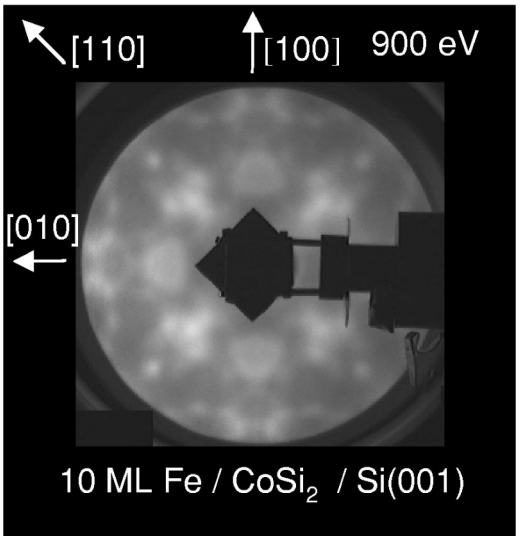

FIG. 3. IMEED pattern for a 10 ML of Fe deposited at RT on a $CoSi_2(001)$ surface taken for a normal incidence electron beam energy of 900 eV.

effect.[21] Therefore, IMEED provides information on local atomic structure in a way very similar to XPD in real space. However, IMEED in contrast with XPD is not chemically selective, since electrons inelastically scattered by atoms of different kinds are superimposed. Figure 3 shows a IMEED pattern, also called Kikuchi pattern, measured for 10-ML Fe deposited at RT onto the $CoSi_2(001)$ surface. The pattern is taken for electron beam at normal incidence with respect to the surface, and at a primary energy $E_p = 900\,\text{eV}$. Only the electrons emitted with polar angles in the 0–40° range are collected by the fluorescent screen. A well-contrasted pattern is observed, which clearly shows a fourfold symmetry as evidenced by strong-intensity modulations. Essentially, the same IMEED pattern is seen at all coverages in the 1–40 ML range and corresponds to the one observed on a Fe(001) single-crystal surface. This immediately indicates that well-ordered films grow on the $CoSi_2(001)$ surface, which adopt a cubic structure.

XPD results

In order to get more specific-site structural information about the evolving structure of Fe films as a function of film thickness, we have employed x-ray photoelectron diffraction (XPD). In XPD, the intensity of a specific core-level photoelectron line is studied as a function of the emission direction. This technique is based on the observation of interferences between the direct photoelectron wave emerging from a specific atom and those waves scattered by neighboring atoms to the emitter. As a result of the interference effects, it is well established[22,23] that at high kinetic energy (several hundred eV) XPD angular distributions of photoelectron-emission intensity have intensity maxima corresponding to the internuclear direction, which connect the emitter atom to its nearest-neighbor scatterer atoms. This mechanism occurs when photoelectron waves emitted by specific atoms are refocused in the forward direction (forward scattering) due to the strong core potential of the atoms neighboring the emitter. XPD does not require the sample to have long-range order, which makes it complementary to LEED, which is routinely used to monitor long-range order in the films.

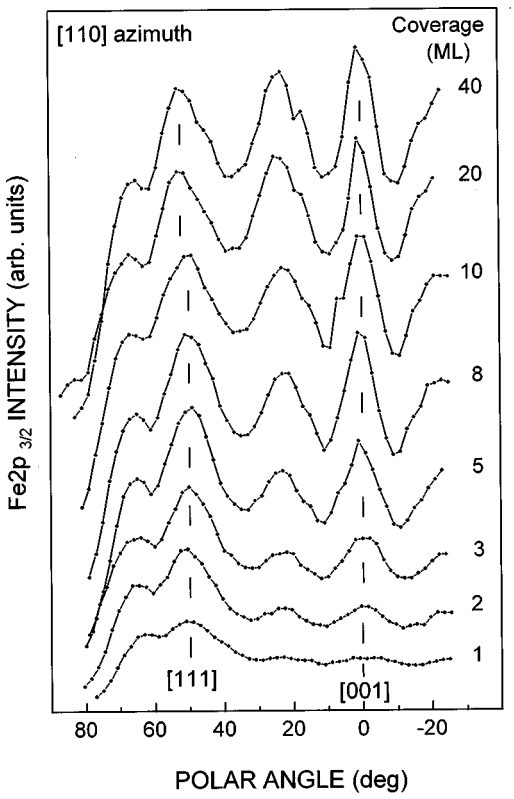

FIG. 4. $Fe2p_{3/2}$ photoelectron intensity angular distributions along the [110] azimuth for increasing thickness of the Fe film on $CoSi_2(001)$. Crystallographic directions correspond to forward scattering at nearest or next-nearest neighbors.

Figure 4 shows the evolution of the intensity angular dependence of $Fe2p_{3/2}$ core level along the [110] azimuth of the Si substrate, as a function of the Fe coverages deposited at RT on the $CoSi_2(001)$. All the photoelectron angular distributions are very similar, with three major peaks clearly identified at polar emission angle around 0°, 23°, and 52°. Along the [100] azimuth only the profile corresponding to 10 ML of Fe is depicted in Fig. 5. It is typical for all the profiles we obtained at various coverages. The major peaks appear at 0°, ~26°, and ~45° polar emission angle. Marked intensity angular modulations with maxima at defined angular positions indicate the formation of an ordered phase. Because Fe is expected to be arranged in a bcc cubic structure, we have reported the corresponding structure model (see inset Fig. 5). According to this accompanying structure model a bcc film would show forward scattering intensity maxima along the [110] azimuth, at normal emission ($\theta = 0°$) and 54.7° polar angle corresponding to beam alignment along the [001] and [111] atomic rows of a bcc phase, respectively. Similarly, along the [100] azimuth, strong enhancement features are expected at 0° and 45° corresponding to the [001] and [101] atomic rows. Thus, it is immediately apparent from these results that Fe most likely grows in a bcc structure whatever the film thickness. Intermediate features at around 25° along the two azimuths are assigned to nonzeroth-order diffraction and scattering by more distant atoms, but are also typical for a bcc local environment. Actually, the presence of peaks visible at normal emission and at ~52° along the [110] direc-

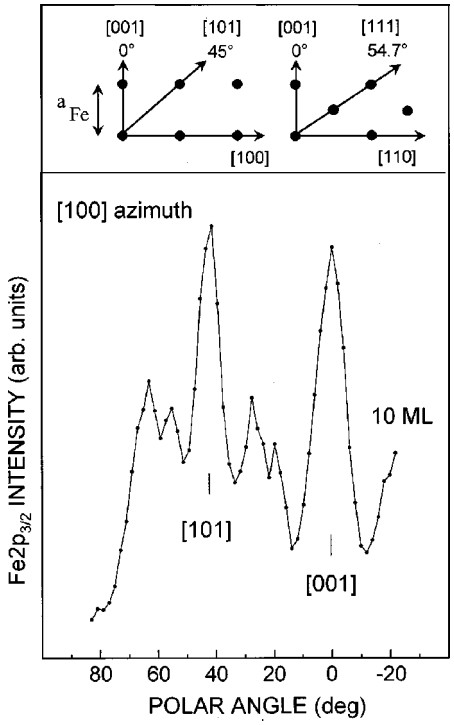

FIG. 5. $Fe2p_{3/2}$ photoelectron intensity angular distributions along the [100] azimuth from a 10 ML-thick Fe film deposited at RT on $CoSi_2$. Crystallographic directions correspond to forward scattering at nearest or next-nearest neighbors. Also shown are the main close-packed atomic directions for a bcc (001) crystal cut along the [110] and [100] symmetry directions.

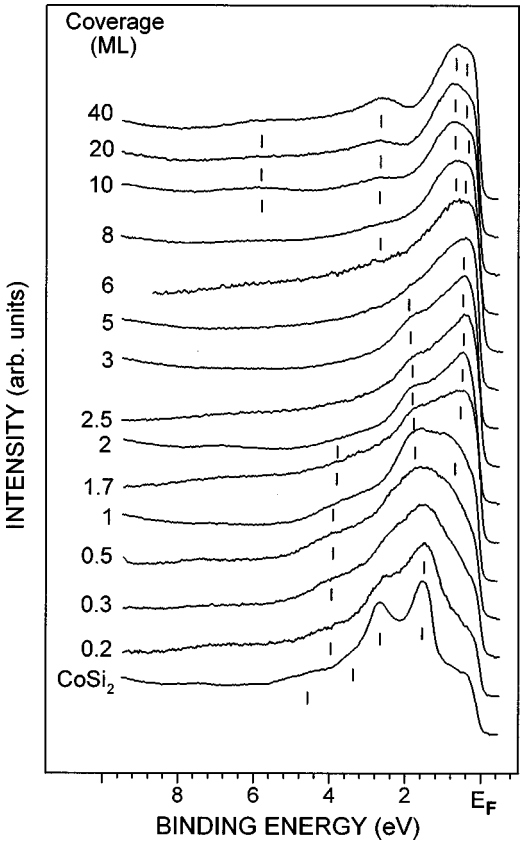

FIG. 6. Angle-resolved photoemission spectra taken at 21.2 eV (He_1) photon energy in normal emission for different thicknesses of Fe overlayers deposited at RT on $CoSi_2$(001).

tion for 1-ML Fe deposit reveals that a fraction of photoelectrons emitted from the Fe are scattered by at least of one and two overlying Fe or Si atoms, respectively, thus giving evidence of multilayer film growth. Consequently, the experimental data for low coverages do not support a simple Fe layer-by-layer growth mode but can be readily explained if intermixing takes place in the early stages of growth, i.e., Fe dissolves at least a part of the Si atoms terminating the $CoSi_2$ layer or if three-dimensional bcc Fe islands are formed.

As can be seen the $Fe2p_{3/2}$ forward scattering peaks at normal emission and at ~52° increase in intensity versus Fe coverage according to the focusing effect as the number of scatterers along the chains becomes larger and reach full intensity after deposition of ~8 and ~5 ML, respectively. The saturation of the forward-scattering peak intensity with increasing film thickness is due to defocusing effect of multiple forward scattering, which appears for a number of scatterers larger than six to eight along close-packed chains in cubic structures.[24] The observed anisotropies measured as (Imax-Imin)/Imax is ~40% for the 0° peak at 8 ML. The presence of this strong forward-scattering peak in the Fe core level also confirms high degree of crystalline order in the deposited layer. The anisotropy as large as 40% is found to be very sensitive to the template layer crystalline quality. Finally, a small shift of the [111] forward-scattering peak (Fig. 4) towards higher polar angles is observed for Fe coverages above ~10 ML. We ascribe this shift to the strain evolution of the Fe films. The Fe overlayers are coherently matched to the $CoSi_2$(001)/Si(001) surface, with the lattice parameter larger ($a_{Fe}=2.86$ Å) than half that of Si ($a_{Si}=5.43$ Å) causing in-plane compression of the Fe lattice at the Fe/$CoSi_2$(001) interface and expansion of the Fe lattice normal to the interface. Thus, this shift indicates that the Fe lattice undergoes a pseudomorphic tetragonal distortion in the thinnest films but relaxes towards its natural bcc form in the thick layers. This result is in good agreement with TEM investigations (see below).

At this point one may thus conclude for Fe deposited on $CoSi_2$(001) surfaces at RT, that even the thinnest films investigated grow epitaxially with a cubic structure. Moreover, the appearance of forward scattering peaks at 0° and 52° along the [110] azimuth for very low coverages (~1 ML) is in line with the fact that either a mixed Fe-Si interface or Fe cluster formation takes place.

ARUPS results

The evolution of the ARUPS spectra yields information on the surface electronic structure and in particular the nature of the bonding between the different species of the probed region. Figure 6 shows typical ARUPS spectra recorded at normal emission geometry ($\theta=0°$) for different thicknesses of RT deposited Fe layers on $CoSi_2$(001) surfaces. The clean $CoSi_2$(001) surface spectrum mainly exhibits two prominent narrow structures at ~1.6 and ~2.8 eV binding energy (BE). They are assigned to the nonbonding states of Co3d electrons in the $CoSi_2$ silicide layer and to surface related states, respectively. The peak attributed to the bonding Co3d-Si3p electron states is located at ~3.5-eV BE. The origin of the

surface states at ~2.8-eV BE is not yet understood. The presence of a such narrow surface-state peak along with strong-angular dependence (not shown here) indicate an excellent crystallinity of the $CoSi_2(001)$ layer in good agreement with the sharp $c(2\times2)$ LEED pattern. After deposition of 0.5 ML of Fe the surface states at ~2.8 eV is quenched and replaced by a broad peak centered at ~1.6 eV. Above 0.5 ML of deposited Fe a second peak develops close to the Fermi level together with a peak at ~1.7 eV. The peak near the Fermi level is assigned to nonbonding Fe $3d$ states while the peak at ~1.7 eV appears to be due to emission from an iron state, which is caused by hybridization effect, i.e., caused by Fe-Si interactions. Hence, for Fe evaporation in the 0–2 ML the ARUPS spectra evolution suggests the formation of a thin-silicide layer at the interface rather then the growth of a pure Fe layer.

In the coverage region between 2 and 6 ML, the spectra are very similar with two prominent peaks at ~0.5- and 1.7-eV BE, respectively. Peak positions and energy separations are very close to those reported for Fe_3Si.[25] However, we can see that the intensity of the peak close to the Fermi level develops in this coverage range. This behavior can be assigned to the growth of unreacted Fe on top of a stable iron-rich phase with composition close to Fe_3Si by the fact that the spectra can be obtained simply as a superposition of pure bcc iron and Fe_3Si spectra. A stoichiometry close to Fe_3Si has also been previously assigned by Gallego *et al.*[8] to the reacted phase formed at the Fe/Si(100) interface. A close inspection of the spectra up to ~2 ML of Fe reveals the presence of a broad structure around 4-eV BE, which may be due to Si $3p$ states reflecting Si segregated on the deposited layer.[26–27] This segregation of Si at low coverage is clearly evidenced by ISS data [Fig. 2(b)].

Above 6-ML thickness, we see that the overall shape of the spectra are similar to each other. Two main structures can be identified at ~0.8- and 2.6-eV BE, respectively, and a broader structure located at ~6-eV BE. The overall shape of the spectra is in very good agreement with published photoemission spectra for clean bcc Fe(001).[28,29] A careful inspection of the structure close to the Fermi level reveals the presence of two components at ~0.3 and ~0.8 eV due to emission from minority-spin Γ'_{25} and majority-spin Γ'_{12} symmetry bands, respectively.[28] The peak at ~2.6 eV corresponds to the emission from majority-spin Γ'_{25} symmetry band. The peak at ~6 eV is attributed to a satellite effect originating from double-d hole state.

Hence, a thin-ordered iron-rich phase is formed at the interface for coverages up to ~2 ML of Fe deposited at RT onto the Si(001) surface. The first Fe atoms react with the surface as testified by the quenching of the $CoSi_2(001)$ surface state and the appearance of new structures in the ARUPS spectra. With increasing Fe coverages, the ARUPS spectra demonstrate that an ordered (1×1) bcc Fe(001) phase begins to grow on the iron-rich-ordered silicide interfacial film, for coverages above ~ 2 ML. The ISS spectra indicate that very small amounts of Si (a few percent of an atomic layer) still persist at the Fe film surface (up to 40 ML) but this is not detectable in the valence-band spectra.

Core-level photoemission results

In order to gain additional information concerning the nature of the chemical bonding states of iron in the layers, we examined the coverage-dependent emission from the Fe$2p_{3/2}$ core-level transition. In Fig. 7 a typical series of normal emission monochromatized Alk_α-excited Fe$2p_{3/2}$ core-level spectra is displayed for increasing Fe coverage on $CoSi_2(001)$ at RT. Also shown for comparison is the spectrum corresponding to a thin $FeSi_2$ layer (~10 Å) epitaxially grown on Si(001). Note that the Fe$2p_{3/2}$ core levels of $FeSi_2$ are within accuracy identical in binding energy to those of FeSi.[26] For coverages up to 8 ML, the Fe$2p_{3/2}$ core-level intensity increases and are progressively shifted towards lower binding energies. This weak shift (~0.1 eV) of the spectra with increasing Fe coverage indicates an increasing Fe coordination of the Fe atoms at or near the interface. Above 8 ML, the energy position is indistinguishable from that of pure bcc Fe. This behavior corresponds to the presence of largely unreacted Fe on top of the reacted interface region. As can be seen in Fig. 7 the binding energy of the Fe$2p_{3/2}$ core levels measured on the deposited layers, are lower by about 0.2–0.3 eV than those of $FeSi_2$ or FeSi silicides even for 1-ML Fe deposit. Thus, it can be concluded that the interfacial reaction product has a higher Fe concentration than FeSi. The relevant energy shifts (~0.2 eV) are actually detected for Fe_3Si with respect to FeSi or $FeSi_2$.[27] These results clearly confirm the ARUPS observations, i.e., at low coverages a chemical interaction between Fe and Si takes place and that an ultrathin iron-rich silicide close to Fe_3Si stoichiometry is formed at the interface.

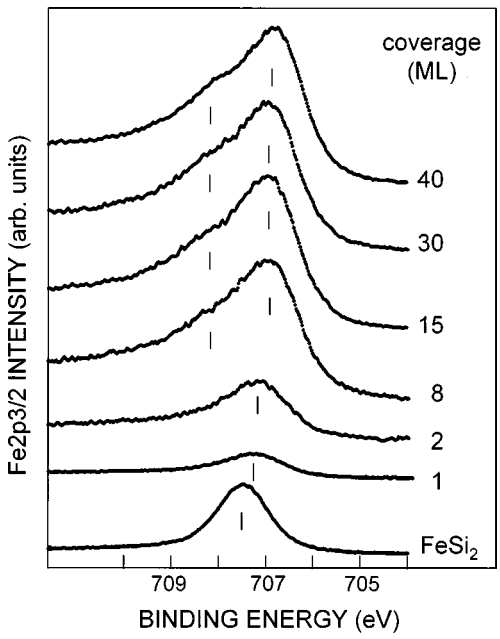

FIG. 7. Fe$2p_{3/2}$ core-level spectra measured for increasing Fe coverages on $CoSi_2(001)$ at RT. The spectra are taken at normal emission using a monochromatized AlK_α source (1486.6 eV). Also shown is the spectrum recorded from a thin $FeSi_2$ (~10 Å) epitaxially grown on Si(001).

Moreover, concerning the Fe$2p_{3/2}$ linewidths, drastic changes are observed. In comparison with the measured Fe$2p_{3/2}$ core-level spectrum of $FeSi_2$ which exhibits only a small asymmetry, typical of metals with an *sp* Fermi surface, the spectra become more and more asymmetric upon increasing the Fe coverage. After deposition of 8 ML the Fe$2p_{3/2}$ line shapes and the binding energy are comparable with the

value previously published in the literature for pure iron.[27] These spectra present an intense tail at high-binding energy of the Fe$2p_{3/2}$ line. This asymmetry in core-level lines can be essentially interpreted as originating from two effects. The first, related to many-body effects is the creation of electron-hole pairs in the valence band simultaneous to core-hole creation. This leads to a small tail at the high-binding energy side of the core lines and is present in all metals. The strength of this asymmetry is chiefly determined by the density and symmetry of the electronic states near the Fermi level. The second effect is originating from the spin and the orbital angular momentum coupling between the core hole and the open valence $3d$ shell that leads to final state multiplet structure in an atomic model.[30] This is the strongest effect of direct relevance here. Previous spin-resolved x-ray photoemission spectroscopy[31] as well as photoemission[32] magnetic circular dichroism (MCD) measurements on the Fe$2p_{3/2}$ have revealed exchange splitting of about 0.5 eV for ferromagnetic Fe due to the atomic moment of 2.2 μ_B. We have recently carried out XPS measurements of the Fe$2p_{3/2}$ core level for epitaxial thick films (100 Å) on Si(111) with compositions ranging from FeSi to Fe.[33] Strong change of the asymmetry versus stoichiometry was observed and interpreted as the result of the evolution of the local magnetic moment in the layers. The shape of the Fe$2p_{3/2}$ for coverages around 2 ML of Fe is very similar to that recorded for the Fe_3Si compound. It is less asymmetric than in pure Fe because of a smaller atomic magnetic moment. We can conclude, as for the core-level shift, that the shape evolution of the Fe$2p_{3/2}$ core level is quite consistent with the ARUPS data, i.e., the initial formation of an Fe_3Si film and growth of essentially pure Fe on top.

TEM results

High-resolution transmission electron microscopy (HRTEM) yields interesting complementary information. It is very appropriate to investigate the coherency of the Fe/Si interface and gain further insight into the epitaxial growth mechanism in this system.

Figure 8 shows cross-sectional HRTEM images along the [110] zone axis and the plane-view diffraction pattern for 10 ML of Fe deposited onto $CoSi_2$(001) at RT. In Figs. 8(a) and 8(b) the dark deposited layer is seen on the Si(001) substrate. We can see that a fairly uniform epitaxial Fe layer is formed on the (001) Si substrate with a sharp Fe/Si interface. The Fe layer is continuous and has an uniform thickness. In Fig. 8(c), the diffraction pattern shows the presence of the diffraction spots from bcc Fe and Si. The diffracted beams common to both systems almost coincide with each other, which indicates that an epitaxial (001) Fe is grown on the Si(001) substrate. The diffraction pattern gives the following orientation relationships Fe(001)⟨001⟩‖$CoSi_2$(001)⟨001⟩‖Si(001)⟨001⟩ in agreement with LEED, IMEED, and XPD measurements. The small difference in spot positions reflects a partially relaxed Fe layer. The ~5.6% lattice mismatch between the Si lattice constant and the Fe lattice constant results in a compression of the Fe lattice at the Fe/$CoSi_2$ interface. For a 10-ML film a strained bcc structure is observed to form. The deposited layer tends to grow pseudomorphically on the $CoSi_2$(001) surface. For thicker film thicknesses (>40 ML) we find that the accumulated misfit strain is essentially released, presumably by introducing point defects or dislocations, the structure evolves to the relaxed bcc Fe(001) phase.

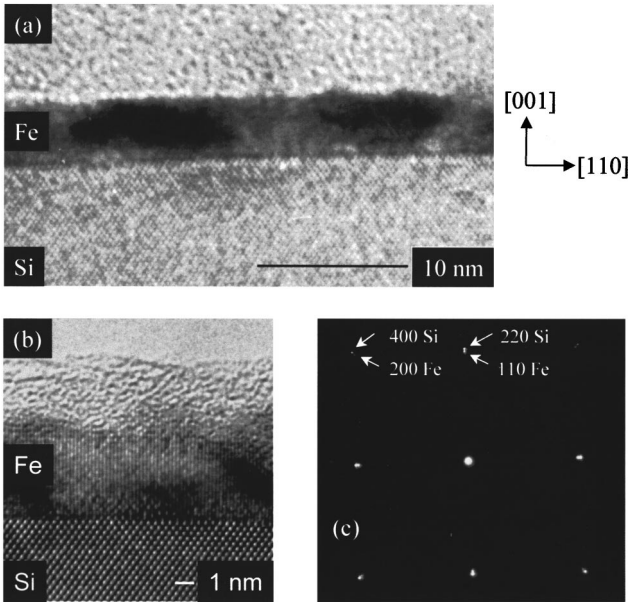

FIG. 8. (a) (b) Cross-sectional high-resolution TEM photographs of a sample with 10 ML of Fe deposited at RT on $CoSi_2$(001)/Si(001) taken along the [110] direction at two different magnifications. (c) Typical plane-view diffraction pattern taken from 10 ML of Fe deposited at RT on $CoSi_2$(001)/Si(001) with the electron beam along the [001] direction. Marked on the diffraction pattern are the 400 and 220 spots from bulk Si reflections along with the 200 and 110 spots from Fe reflections.

IV. CONCLUSION

In this study, we have proposed a procedure for the growth, at RT, of epitaxial ultrathin bcc Fe(001) films on Si(001), by using an epitaxial thin $CoSi_2$(001) template layer that prevents the interdiffusion of the Si through the Fe overlayer. The $CoSi_2$(001) seed layer has permitted the growth of epitaxial as opposed to polycrystalline ultrathin Fe layers on Si(001) in the thickness range 0–40 ML. At low coverages ($\leqslant$ 2 ML) an ordered epitaxial Fe-rich interfacial layer having a composition close to Fe_3Si is formed. On top of this reacted stable layer, growth of well-ordered essentially pure bcc Fe(001) layers occurs with small Si surface segregation visible at coverages up to 40 ML. The use of such a template both blocks the reaction with the Si substrate and permits epitaxial growth of the Fe in the form of sharp heterostructures or multilayers. Preliminary results indicate that such ultrathin epitaxial Fe films present magnetic anisotropies strongly modified by interfacial effects when compared to those in the respective bulk material. MOKE investigations to be published elsewhere[34] indicate that ordered (001) Fe layers stay ferromagnetic down to coverages around 4 ML at RT. Moreover, we observe that the use of an epitaxial $FeSi_2$ silicide template layer (~10 Å) prepared by deposition of ~4 ML of Fe and subsequent annealing to 550 °C also results in the growth of well-ordered bcc Fe(001) layers at RT.

*Author to whom correspondence should be addressed. FAX: 03 89 33 60 89. Electronic address: P.Wetzel@univ-mulhouse.fr

[1] J. J. de Vries, J. Kohlhepp, F. J. A. den Broader, R. Coehoorn, R. Jungblut, A. Runders, and W. J. M. de Jonge, Phys. Rev. Lett. **78**, 3023 (1997).
[2] A. Chaiken, R. P. Michel, and M. A. Wall, Phys. Rev. B **53**, 5518 (1996).
[3] L. M. Alvarez-Prado, G. T. Perez, R. Morales, F. H. Salas, and J. M. Alameda, Phys. Rev. B **56**, 3306 (1997).
[4] Y. Endo, O. Kitakami, and Y. Shimada, Phys. Rev. B **59**, 4279 (1999).
[5] R. Kläsges, C. Carbone, W. Eberhardt, C. Pampuch, O. Rader, J. Kachel, and W. Gutat, Phys. Rev. B **56**, 10 801 (1997).
[6] J. Alvarez, J. J. Hinarejos, E. G. Michel, G. R. Castro, and R. Miranda, Phys. Rev. B **45**, 14 042 (1997).
[7] K. Rührnshopf, D. Borgmann, and G. Wedler, Thin Solid Films **280**, 171 (1996).
[8] J. M. Gallego, J. M. Garcia, J. Alvarez, and R. Miranda, Phys. Rev. B **46**, 13 339 (1992).
[9] Z. H. Nazir, C.-K. Lo, and M. Hardiman, J. Magn. Magn. Mater. **156**, 435 (1996).
[10] D. Berling, G. Gewinner, M. C. Hanf, K. Hricovini, S. Hong, B. Loegel, A. Mehdaoui, C. Pirri, M. H. Tuilier, and P. Wetzel, J. Magn. Magn. Mater. **191**, 331 (1999).
[11] R. T. Tung, J. C. Bean, J. M. Gibson, J. M. Poate, and D. C. Jacobson, Appl. Phys. Lett. **40**, 684 (1982).
[12] L. Haderbache, P. Wetzel, C. Pirri, J. C. Peruchetti, D. Bolmont, and G. Gewinner, Phys. Rev. B **39**, 1422 (1989).
[13] J. Henz, M. Ospelt, and H. von Känel, Surf. Sci. **211–212**, 716 (1989).
[14] D. Loretto, J. M. Gibson, and S. M. Yalisove, Phys. Rev. Lett. **63**, 298 (1989).
[15] J. R. Jiminez, L. M. Hsiung, K. Rajan, and J. L. Schowalter, Appl. Phys. Lett. **116**, 2811 (1990).
[16] S. M. Yalisove, R. T. Tung, and D. Loretto, J. Vac. Sci. Technol. A **7**, 1472 (1989).
[17] R. Stalder, C. Schwarz, H. Sirringhaus, and H. von Känel, Surf. Sci. **271**, 355 (1992).
[18] W. Weiss, U. Starke, K. Heinz, G. Rangelov, T. Fauster, and G. R. Castro, Surf. Sci. **347**, 117 (1996).
[19] M. Henzler, Surf. Rev. Lett. **4**, 489 (1997).
[20] P. Hahn, J. Clabes, and M. Henzler, J. Appl. Phys. **51**, 2079 (1980).
[21] S. A. Chambers, Surf. Sci. Rep. **16**, 261 (1992).
[22] C. S. Fadley, Prog. Surf. Sci. **16**, 275 (1984).
[23] W. F. Egelhof, Jr., Crit. Rev. Solid State Mater. Sci. **16**, 213 (1990).
[24] M. L. Xu, J. J. Barton, and M. A. Van Hove, Phys. Rev. B **39**, 8275 (1989).
[25] H. Busse, J. Kandler, B. Eltester, K. Wandelt, G. R. Castro, J. J. Hinarejos, P. Segovia, J. Chrost, E. G. Michel, and R. Miranda, Surf. Sci. **381**, 133 (1997).
[26] B. Egert, H. J. Grabke, Y. Sakisaka, and T. N. Rhodin, Surf. Sci. **141**, 397 (1984).
[27] B. Egert and G. Panzner, Phys. Rev. B **29**, 2091 (1984).
[28] A. M. Turner, A. W. Donoho, and J. L. Erskine, Phys. Rev. B **29**, 2986 (1984).
[29] M. Pessa, P. Heimann, and H. Neddermeyer, Phys. Rev. B **14**, 3488 (1984).
[30] D. Shirley, in *Topics in Applied Physics*, *Photoemission in Solid I*, edited by M. Carbona and L. Ley (Springer-Verlag, Berlin, 1978), p. 165.
[31] D. G. Van Campen, R. J. Pouliot, and L. E. Klebanoff, Phys. Rev. B **48**, 17 533 (1993).
[32] L. Baumgarten, C. M. Schneider, F. Petersen, H. Schäfers, and J. Kirschner, Phys. Rev. Lett. **65**, 492 (1990).
[33] S. Hong, U. Kafader, P. Wetzel, G. Gewinner, and C. Pirri, Phys. Rev. B **51**, 17 667 (1995).
[34] P. Bertoncini, D. Berling, A. Mehdaoui, P. Wetzel, B. Loegel, and G. Gewinner (unpublished).